Researchers Journal of Science and Technology (REJOST)

https://rejost.com.ng

Structural, Electronic, Thermophysical and Optical Investigation of Tetragonal ($C11_b - CrSi_2$) Material: A Theoretical Analysis

E. J. Ekwere, J. B. Emah, S. A, Ekong*

Received: May 19, 2024 /Accepted: July 25, 2024

Abstract

Chromium disilicide ($CrSi_2$) have garnered significant attention owing to the novel functions and considerable prospective it holds in ultrahigh temperature engineering applications. The tetragonal structure ($C11_b - CrSi_2$) being one of the polymorphs of the $CrSi_2$ is investigated in this paper for its thermophysical and optical dielectric properties, which are still lacking in reported studies. The present investigation aim to study the optical real and imaginary parts of dielectric function, joint density of state, the refractive index, and extinction coefficient using first-principle calculations based on density functional theory (DFT). This approach requires knowledge of the atomic species and crystal structure to predict several physical properties of materials. The values of the optimized lattice parameters are in good agreement with experimental results. The diagrams illustrating the electronic band structure and density of state (DOS) plots reveal the compound from the bonding and antibonding characters as a metal in accordance with the experiment. The calculated DOS of tetragonal $C11_b - CrSi_2$ is 3.61 per eV. In addition, while the equilibrium unit-cell volume, bulk modulus B_0, and bond-lengths (Si–Si and Cr–Si) are in agreement with the available data, the first derivative of the bulk modulus and minimum energy are predicted for future studies. Furthermore, the thermophysical properties of the compound are analyzed at 300 K. The evaluated Debye temperature $\theta_{(D)}$ (= 867.87 K) and the high value of B_0 (= 284.0 GPa) reflect the feasibility of the material being ductile, while the Debye heat capacity (142.13 J/mol·K) reveals the Dulong-Petit limit. Also, we predict a minimum thermal conductivity of 17.43 mW/K/m. Our study shows that the internal energy, the entropy, and the constant volume heat capacity increase with increasing temperature, while the free energy decreases monotonously with the increase in temperature. Consequently, predictive models for the thermodynamic quantities are herein presented. The calculated optical dielectric properties, such as imaginary and real parts of dielectric function, refractive index, and extinction coefficient, reveal relatively high anisotropy, with indications that the absorption spectrum predominantly depends on the electronic transitions from 3d-Cr and 3p-Si migrations around the Femi level.

✉ S. A, Ekong: sylvesterekong@aksu.edu.ng

Department of Physics, Akwa Ibom State University, Ikot Akpaden, P.M.B. 1167, Uyo, Nigeria

Keywords: Chromium disilicide; Tetragonal $C11_b - CrSi_2$; Dielectric functions; DOS; Thermodynamic properties

1.0 Introduction

Recently, there has been accelerated interest in studying transition-metal (TM) disilicides due to their broad advances in areas of engineering and sciences, which cut across thermo-electricity, energy-storage systems, and high-temperature device applications. Silicon (Si) in combination with TM and other elemental constituents have been an active area of research over the years as it plays crucial roles in advancing technology in areas of quantum confinement, nanostructures, optoelectronics, photoelectronics, photo-electrics, etc. (Mousa *et al*., 2015, Maier-Flaig *et al*., 2013, Yate *et al*., 2017, Ekong *et al*., 2014; 2015; 2016, Cheng *et al*., 2013). Of the various TM disilicides(Si_2), which include the Molybdenum-based disilicides (Yakaboylu *et al*., 2020), Tungsten disilicides (Xiong *et al*., 2020), and Niobium-based disilicides (He *et al*., 2020), investigations on the Chromium-based disilicides ($CrSi_2$) have received growing interest owing to the recent discovery of two new structural phases. Nevertheless, Niobium-based disilicides ($NbSi_2$) are remarkable for ultrahigh-temperature systems because they exhibit fascinating high-temperature strength with good thermal stability (He *et al*., 2020). Tungsten disilicides (WSi_2) reveals excellent thermoelectricity technology, which are useful in renewed thermoelectric devices (Xiong *et al*., 2020). Molybdenum-based disilicides ($MoSi_2$) stand out as energy-storage materials for excellent electronic properties (Yakaboylu *et al*., 2020). Manganese disilicides ($MnSi_2$) are polytypes in nature and show possible half-metallicity, robust characteristics of degeneracy, exhibit helimagnetism below critical temperature (T_C), and a resulting maximum power factor of $5.6 \times 10^{-4}\, W/K^2m$ (Shin *et al*., 2015). Iron disilicides (β-$FeSi_2$) being a low temperature phase, are applauded for thermoelectric generation of high thermo-electric power and resistance to oxidation, and can easily form thermocouples, that consist of both n- and p-type β-$FeSi_2$, which find usefulness in changing heat to electrical energy (Kondo *et al*., 1994). Chromium disilicides ($CrSi_2$) depict high electrical conductivity, strong oxidation resistance, high thermal stability, as well as growing intrigues in areas of microelectronics and photoelectron tech-nology (ShiYun *et al*., 2009). From a dichalcogenide viewpoint, two-dimensional (2D) magnetic monolayers of $TMSi_2$ materials were reported for potential applications in spintronics and magnetic storage devices (Han *et al*., 2015). According to them, the formation energies of ferromagnetic $TiSi_2$ and antiferromagnetic $FeSi_2$ monolayers are found to be lower than those of silicone, whereas a large magnetic moment of 2.512 μ_B per Mn atom was reported for the monolayer $MnSi_2$ sheet.

Nevertheless, although the structural and physical properties of $CrSi_2$ silicide have been extensively studied, there are few reported studies at present on the optical properties of hexagonal C40 structure, yet none to the best of our knowledge on tetragonal $C11_b$ structure except the absorption coefficient reported by Pan (2020b). Moreover, materials optical properties are mainly described by dielectric functions, refractive index, extinctive coefficient, absorption coefficient, optical conductivity, etc., which are determined from band structure, carrier concentration, and mobility near the Fermi surface. Therefore, this

necessitates the aim of the present investigation on the tetragonal $C11_b$ structure, which studies the optical real and imaginary parts of dielectric functions, joint density of state, the refractive index, and extinctive coefficient of this photoelectric material. In this article, the nature of the reported optical properties has important significance for plasmon applications. The purpose of the current article is to further our understanding of the sensitivity and resilience of the tetragonal $C11_b$ structure of $CrSi_2$ when subjected to photons.

2.0 Computational Details

The optimization of the geometrical structure and calculation of thermal properties were performed using the first-principles density functional theory approach as implemented in quantum espresso code (Giannozzi *et al*., 2009). The exchange and correlation potentials are described using generalized-gradient approximation (GGA) in the parameterization of the Perdew–Burke–Ernzerhof (PBE) functional scheme (Vanderbilt, 1990). The interactions between the valence electrons and ion core were as described by the ultra-soft pseudo-potentials. The atomic configurations used to generate the ultra-soft pseudo-potentials are $3d^5\ 4s^1$ for Cr and $3s^2\ 3p^2$ for Si, respectively. To ensure the convergence of our calculations, we have tested the cutoff energy and *k*-point grid. The energy cutoff of 720 Ry for plane wave expansion and the Brillouin-zone sample of 9 x 9 x 4 *k*-points would ensure the self-consistent convergence. All the calculations converge with the energy and force tolerance criterion of 10^{-6} Ry and 1×10^{-4} Ry/Å, respectively. A k-point sampling of 14 x 14 x 6 is set in the Brillouin zone integrations based on the Monkhorst–Pack scheme (Monkhorst and Pack, 1976) for tetrahedron calculations. To analyze the thermodynamic quantities, the thermo_pw code (Malica and Corso, 2020) is used. Importantly, calculations of the optical response functions to electromagnetic waves were performed using the linear-response method within norm-conserving pseudopotential.

3.0 Results and Discussion

3.1 Structural and Electronic Properties

The crystallographic structure of $CrSi_2$ belongs to the conventional body-centered tetragonal unit-cell, which crystallizes in the P4/mmm (No. 123) space group for the $C11_b$ phase. The structure consists of six atoms per unit-cell volume, where the atomic configurations Cr: [Ar] $3d^5\ 4s^1$ and Si: [Ne] $3s^2\ 3p^2$, which occupy the Wyckoff sites of (0, 0, 0) and (0, 0, 0.3368) with crystal angles at $\alpha = \beta = \gamma = 90^0$ respectively. At the crystal edges of Figure 1(c), there is tetrahedral bonding of Cr atoms to a base-centered Si atom, while the body-centered Cr atom forms an octahedral bond with eight Si atoms. The formation of the Cr–Si bonds and Si–Si bonds are resultant effect of the hybridization of the Cr –Si atoms and Si−Si atoms respectively. Moreover, the presence of the bonds enhances the stability of the $C11b - CrSi_2$ alloy. The calculated bond lengths for Cr−Si and Si−Si from our optimization are as given in Table 1. By performing series of self-consistent field (SCF) calculations using the converged energy cutoff and k-points, various total energy with their corresponding unit-cell volume are obtained due to lattice parameters optimization. The plot of the calculated total energy (E) for the $C11_b - CrSi_2$ structure as a function of the unit-cell volume (V_0) within the GGA approximations is as displayed in Figure 1(a). By fitting the illustrated total energy versus unit-cell volume (E-V_0) data sets plotted in Figure 1(a), it was possible to obtain the static structural properties like the bound state energy E_0, the bulk modulus B_0,and the first derivative of the bulk modulus B_P at zero pressure $(P = 0)$. The procedure consisted of fitting the (E-V) data by using the Murnaghan equation of state (EOS) (Murnaghan, 1944).

$$E(V) = E_0 + \frac{B_0}{B_P(B_P-1)}\left[V\left(\frac{V_0}{V}\right)^{B_P} - V_0\right] + \frac{B_0}{B_P}(V - V_0) \quad (1)$$

From the fitted data, eigenvalues of the E_0, B_0 and B_P were recorded as -395.31 Ry, 284.0 GPa and 454, respectively. The results gotten from our optimized lattice parameters ($a_0 = 3.056$ Å and $c_0 = 7.446$ Å), and the bulk modulus B_0 are summarized in Table 1, in comparison with the experiment (Pan *et al*., 2019) and theoretical data by other authors. The calculated results of the lattice parameters are in excellent accord with the ones from the experiment ($a_0 =$ 3.085 Å, and $c_0 = 7.485$ Å) measured at ambient conditions (Pan *et al*, 2019). The calculated lattice parameters of a_0 and c_0 within the GGA underestimate the experimental values by 2.9% and 3.9%, respectively. Our values of a_0 and c_0 are the equilibrium lattice constants from the optimized structure. The value of B_0 (284.0 GPa) obtained in this study is in good accord with the theoretical value obtained from the elastic constants C_{ij} reported by Pan (2020). Obviously, it is found that the slight variations in the calculated lattice parameters lead to a reduction of $C11_b - CrSi_2$ disilicide unit-cell volume when compared with other theoretical data. However, this reduction is attributed to the resulting large bulk modulus, which could be due to compaction.

In Figure 2, a display of the electronic band structure and total density of state (Total-DOS) plots of the $C11b - CrSi_2$ alloy is illustrated. The red-dash line in Figure 2(a) at 0 eV is the Fermi energy (E_F) level that separates the valence band from the conduction band. The illustrated band structure is depicted along the high symmetry points Γ → X → M → Γ → X → R → A → Z → X → R → M → A. We notice at this instant that the upper-most valence bands and the lowest conduction bands overlap at their respective symmetries. Consequently, no energy gap is present around the Fermi level (E_F), which is an indication of a metallic state in the $C11_b - CrSi_2$ alloy. The origin of this metallic character has previously been detailed in a report by Pan (2020), and our resulting electronic structure is equivalent to and resembles the situation described therein. However, the vertical profile of the energy bands corroborates the results of our calculated Total-DOS depicted in Figure 2(b). The horizontal dashed red line marks the critical value for the Total-DOS at E_F. The Total-DOS plot is composed of the admixture between dominant Cr 3d- and Si 3p-states, with smaller contributions from Si 3s-states. This attribute is mainly from the p-d hybridization of the Si and Cr atoms. The valence band in both plots can be sectionalized into two regions within the ranges of – 4.0 to – 14.0 eV (lower region) and +0.0 to – 4.0 eV (upper region), respectively. The lower region is the 3s–3p contributions from Si atoms where the charge interaction forms the Si–Si bonds. The upper region consists of the 3d–3p states where the charge interaction forms Cr–Si bonds. In addition, the uppermost region (+0.0 to +6.0 eV) is the Cr–Si antibonding state, consisting of interactions from the Cr-d, Si-p, and Si-s states. The non-indication of energy gap at the Fermi level shows the material's metallicity, with the antibonding e_g-zone predominantly dominated by 3d–3p states from the t_{2_g} states. The bonding and antibonding characters favour the electrical transportation property as well as the carrier-type of the alloy, which is decided mainly by the Cr-d and Si-p electron layers. The calculated DOS around the Fermi level is 3.61 per eV.

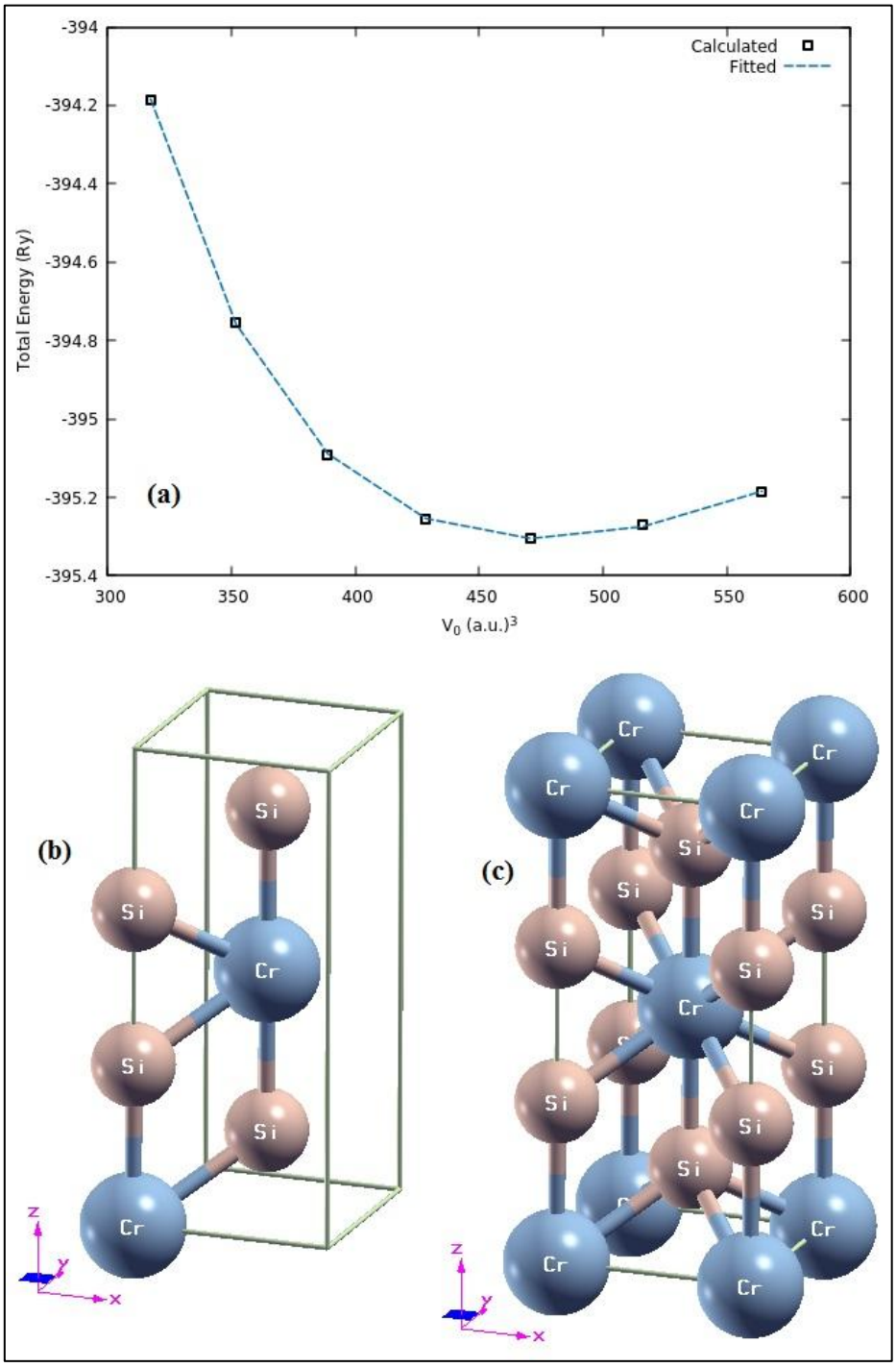

Figure 1: (a) Plot of Total energy (in Ry) versus V_0 (in cubic a.u.) for the $C11_b - CrSi_2$ alloy (b) Translational symmetry of the unit-cell volume and **(c)** Crystal structure of the $C11_b - CrSi_2$ material

3.2 Thermophysical Properties

3.2.1 Thermal Conductivity

In the complexity of several materials, electrons do not partake in the conduction process as only phonon conductions are expected (Lebga *et al.*, 2018). Thermal conductivity is an important thermophysical property that measures the thermoelectric ability of a material to conduct heat. Thus, in order to know the candidacy of a material for thermoelectric application, the minimum thermal conductivity (k_{min}) required is calculated. The minimum thermal conductivity can be evaluated under the assumption that lattice thermal conductivity in glasses and complex crystals can approach k_{min} at

relatively low temperature, when compared with the melting temperature at which the k_{min} is reached for simple crystal structures (Jong *et al.*, 2016).

The calculated value of k_{min} for the mentioned binary alloy ($C11_b - CrSi_2$) was performed using the model proposed by Clarke (2003), according to the relation:

$$k_{min} = k_B V_{avg.} \left(\frac{M_m}{n\rho N_A}\right) \quad (2)$$

and

$$V_{avg} = \left(\frac{1}{3}\left[\frac{1}{V_C{}^3} + \frac{2}{V_S{}^3}\right]\right)^{-1/3} \quad (3)$$

where k_B is Boltzmann's constant, $V_{avg.}$ is the average sound velocity, N_A is Avogadro's number, ρ is the density, M_m is the molecular weight, n is the number of atoms, while V_C and V_S are compressional and shear sound (or elastic wave) velocities (Anderson, 1963, Gregory et al., 2024) for the polycrystalline material.

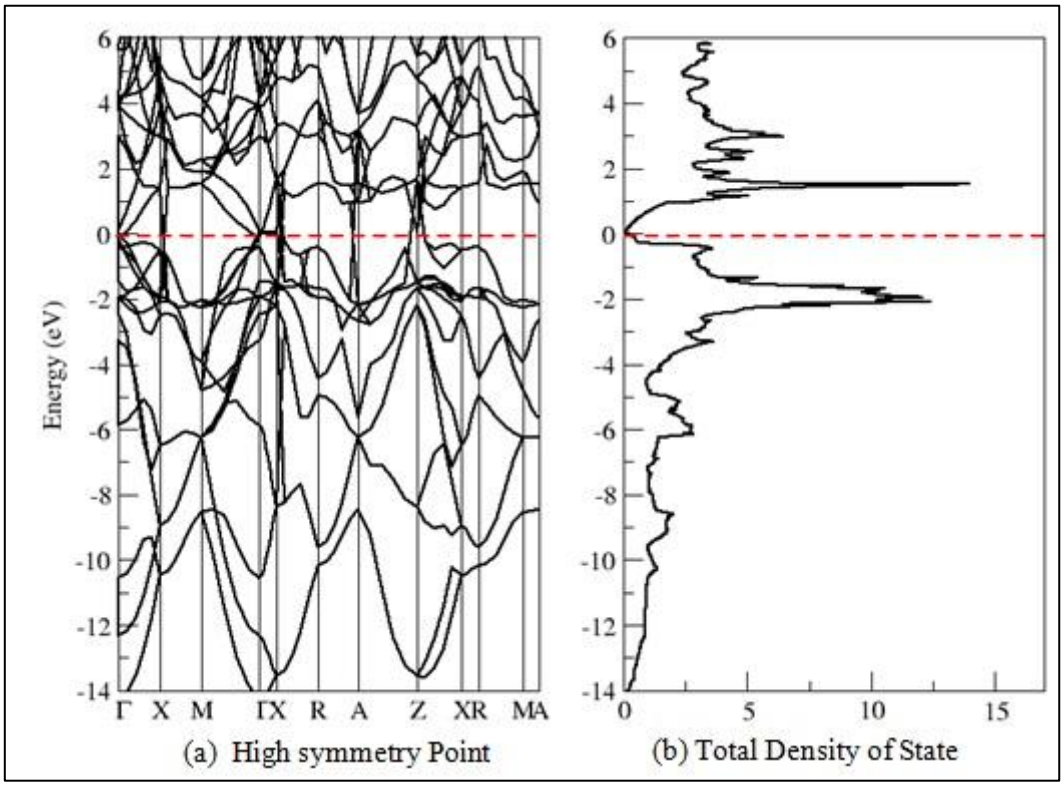

Figure 2: Electronic band structure and total density of state of $C11_b - CrSi_2$. The red-dotted line denotes the Fermi energy (F_E) level

Table 1: Optimized lattice parameters a_0 (Å) and c_0 (Å), bulk modulus B_0 (GPa), first derivative of bulk modulus B_P (GPa), unit-cell volume V_0 (Å^3), minimum energy E_0 (Ry) Si–Si bond length (Å) and Cr–Si bond length (Å) of $C11_b - CrSi_2$.[(a)] Mattheiss (1992), [(b)]Pan (2020)

Tetragonal $C11b - CrSi_2$	a_0	c_0	c_0/a_0	B_0	B_P	V_0	E_0	Si–Si bond	Cr–Si bond
Present work	3.056	7.446	2.437	284.000	4.540	70.270	-395.305	2.441 & 2.460	2.471
[(a)]Experiment	3.085	7.485	2.426	-	-	-	-	-	-
[(b)]Theory	3.079	7.524	2.444	200.910	-	71.300	-	2.458 & 2.538	2.533

Moreover, in metals and semiconductors, the conduction process is predominated by electronic contribution. Using the above relation, the phonon contribution to thermal conductivity (k_{min}) is as presented herein. The calculated k_{min} value for the tetragonal $CrSi_2$ compound is analyzed and our numerical estimate of k_{min} at zero pressure for the material is given in Table 2. The low thermal conductivity value recorded in this study for the $C11_b - CrSi_2$ alloy is evident that the material is promising for applications in thermoelectric technology. Meanwhile, the thermal conductivity of a material measures how well such materials can conduct heat, and it is directly linked to its specific heat because materials with higher specific heat yield higher thermal conductivity. Moreso, materials resulting from complex molecular structures will offer better transfer of heat energy between particles. Unfortunately, until now, literature has no data available to compare this property for the tetragonal $C11_b - CrSi_2$ compound. Therefore, our calculated value for k_{min}can be considered a prediction, thus paving the ways for future comparison from other theoretical calculated results.

3.2.2 Other Thermodynamic Properties

As a fundamental parameter, Debye temperature (θ_D) is of great importance to realizing specific physical properties dovetailing modern chemistry with physics and experiments along with first-principles calculations. These physical properties are not constrained to specific heat, thermal conductivity, melting temperature, etc. Moreover, thermal properties play vital roles in thermoelectric engineering applications. Thermodynamic properties of crystals are generally described from Debye temperature (θ_D) formalism by following the expression (Anderson, 1963):

$$\theta_D = \frac{h}{k_B}\left[\frac{3n}{4\pi}\left(\frac{N_A\rho}{M_m}\right)\right]^{\frac{1}{3}} V_{avg.} \qquad (4)$$

The current investigation evaluates the vibrational mean (or internal) energy ($U_{Int.}$), free energy (F_{Vib}), constant volume heat capacity (C_V) and entropy (S) with respect to temperature variations up to 800 K shown in Figure 3. In the same order, the mentioned quantities are calculated from the given equations (Malica *et al.*, 2020; Pan, 2020):

$$U_{Int.} = \frac{1}{n}\sum_{q,\delta}\frac{\hbar\omega_\delta(q,\delta)}{2} + \frac{1}{n}\sum_{q,\delta}\frac{\hbar\omega_\delta(q,\delta)}{exp(\hbar\omega_\delta(q,\delta)/k_BT)-1} \qquad (5)$$

$$F_{Vib} = \frac{1}{2n}\sum_{q,\delta}\hbar\omega_\delta(q,\delta) + \frac{k_BT}{n}\sum_{q,\delta} ln\left\{1 - exp\left(\frac{-\hbar\omega_\delta(q,\delta)}{k_BT}\right)\right\} \qquad (6)$$

$$C_V = \frac{k_B}{n}\sum_{q,\delta}\{\beta\hbar\omega_\delta(q,\delta)\}^2 \times \left\{exp.\left(\beta\hbar\omega_\delta(q,\delta)\right)/[exp.\{\beta\hbar\omega_\delta(q,\delta)\} - 1]^2\right\} \qquad (7)$$

$$S = -k_B\sum_{q,\delta} ln\left\{1 - exp\left(-\beta\hbar\omega_\delta(q,\delta)\right)\right\} - \frac{1}{T}\sum_{q,\delta}\{\beta\hbar\omega_\delta(q,\delta)/(exp.\{\beta\hbar\omega_\delta(q,\delta)\} - 1)\} \qquad (8)$$

where n is the number of particles in the crystal, $\hbar$ is the reduced Planck constant, k_B is Boltzmann constant, $\hbar\omega_\delta$ is the photon energy, and T is the temperature of the tetragonal $CrSi_2$ compound. The summation in the equations runs over the phonon frequencies $\omega_\delta(q,\delta)$, where q denotes the wave vectorsin the Brillouin zone and δ denotesthe different phonon modes. Within a quasi-harmonic approximation, the vibrational energy influences greatly the properties of the material. An increase in the vibration strength of a material generally can lead to a deviation in the crystal stacking thereby resulting in the decreased moduli of elasticity in the studied compounds. Thus, from Figure 3(a), it is observed that the internal energy of $C11_b - CrSi_2$ remains constant at temperatures from zero ($49.26kJmol^{-1}$) to circa

100 K, and then increases monotonically at higher temperatures. Similar to the internal energy, the free energy F_{Vib} as depicted in Figure 3(b), retained its value of 48.63 $kJmol^{-1}$ at 0K up to 100 K, and thereafter decreases monotonically with increasing temperatures up to 800 K. Meanwhile, at 799 K the F_{Vib} is recorded as $-26.52kJmol^{-1}$. It is noticed that at zero-temperatures, both the internal energy and free energy are relatively of the same energy value. This implies that as the temperature, increases the ability for the material to retain energy in the form of heat reduces, thus making it suitable for high temperature applications. Furthermore, illustrated in Figure 3(c) is the isochoric heat capacity C_V dependence on temperature T, for the $C11_b - CrSi_2$ alloy at zero-pressure. The plot depicts the exponential increase of C_V at T < 600 K. However, it approaches the Dulong-Petit limit at higher temperatures, which is a constraint that allows all phonon modes to reach sufficient excitations due to thermal energy (Bioud *et al*., 2017). Evidently, the $C11_b$ structure reveals a Dulong-Petit limit of 142.13 J/(K-mol) for C_V (heat capacity) which is way higher than the 72.0 J/(K-mol) reported for the hexagonal-C40 structure (Lu *et al*., 2021). This is an indication showing the tetragonal $C11_b$ structure is a better shielding device than the C40 (hexagonal) structure in the ultraviolet region, and can serve better for device and automobile coatings due to its tendency as a heat or light absorber. Moreso, at low temperatures the vibration excitations generate acoustic vibrations. At 300 K, the entropy S due to vibration is found to be $67.84\ Jmol^{-1}K^{-1}$. It is noticed from the graphs that similar qualitative behaviors have been reported in related compounds (Pan *et al*., 2017, Lu *et al*., 2021) for the T-dependence of $U_{Int.}$, F_{Vib} , S and C_V respectively. The predictive models obtained in our work by fitting the graphs for correlation between the mentioned thermodynamic quantities follow the polynomial functions given in equations ((9) – (12)):

$$U_{Int.} = 49.26 - 0.28 \times 10^{-1}T + 0.03 \times 10^{-2}T^2 + 4.00 \times 10^{-9}T^3 - 4.00 \times 10^{-10}T^4 + 2.00 \times 10^{-13}T^5 \quad (9)$$

$$F_{Vib} = 48.63 + 0.24 \times 10^{-2}T + 2.00 \times 10^{-5}T^2 - 5.00 \times 10^{-7}T^3 + 7.00 \times 10^{-10}T^4 - 3.00 \times 10^{-13}T^5 \quad (10)$$

$$C_V = (379.07 - 37.79T) \times 10^{-2} + 0.79 \times 10^{-2}T^2 - 3.00 \times 10^{-5}T^3 + 6.00 \times 10^{-8}T^4 - 5.00 \times 10^{-11}T^5 + 2.00 \times 10^{-14}T^6 \quad (11)$$

$$S = (228.65 - 16.31T + 0.25T^2) \times 10^{-2} - 6.00 \times 10^{-6}T^3 + 5.00 \times 10^{-9}T^4 - 2.00 \times 10^{-12}T^5 \quad (12)$$

Nevertheless, worthy of note is that at zero pressure and zero temperature, the Debye temperature (θ_D) of the $C11_b - CrSi_2$ structure is larger than that of other transition metal disilicides with higher molecular weights (Wan *et al*., 2016, Pan *et al*., 2017, Vasudévan *et al*., 1992). Reports from literature have it that higher Debye temperature reflects lower atomic mass, as well as short interatomic bond length (Bioud *et al*., 2017; Adachi, 2005). The obtained values of our studied thermodynamic quantities for the $C11_b - CrSi_2$ alloy as presented in Table 2 include the mass density, thermal conductivity, specific heat capacity at constant volume, the Debye temperature, the zero-point energy, and the ultrasonic parameters (sound velocities), respectively. Both the Debye temperature and thermal conductivity are obtained in relation to expressions containing the average sound velocity. Between the Debye temperature, specific heat capacity, and thermal conductivity, the behavior of one predetermines the proportionate behavior of the other. The specific heat capacity graph of this alloy satisfies the T^3 law at low temperatures and retains the Dulong–Petit law at high temperatures. Moreover, the high-temperature thermodynamic behavior of this disilicide is highly dependent on the lattice vibrations of Si and Cr–Si bonds.

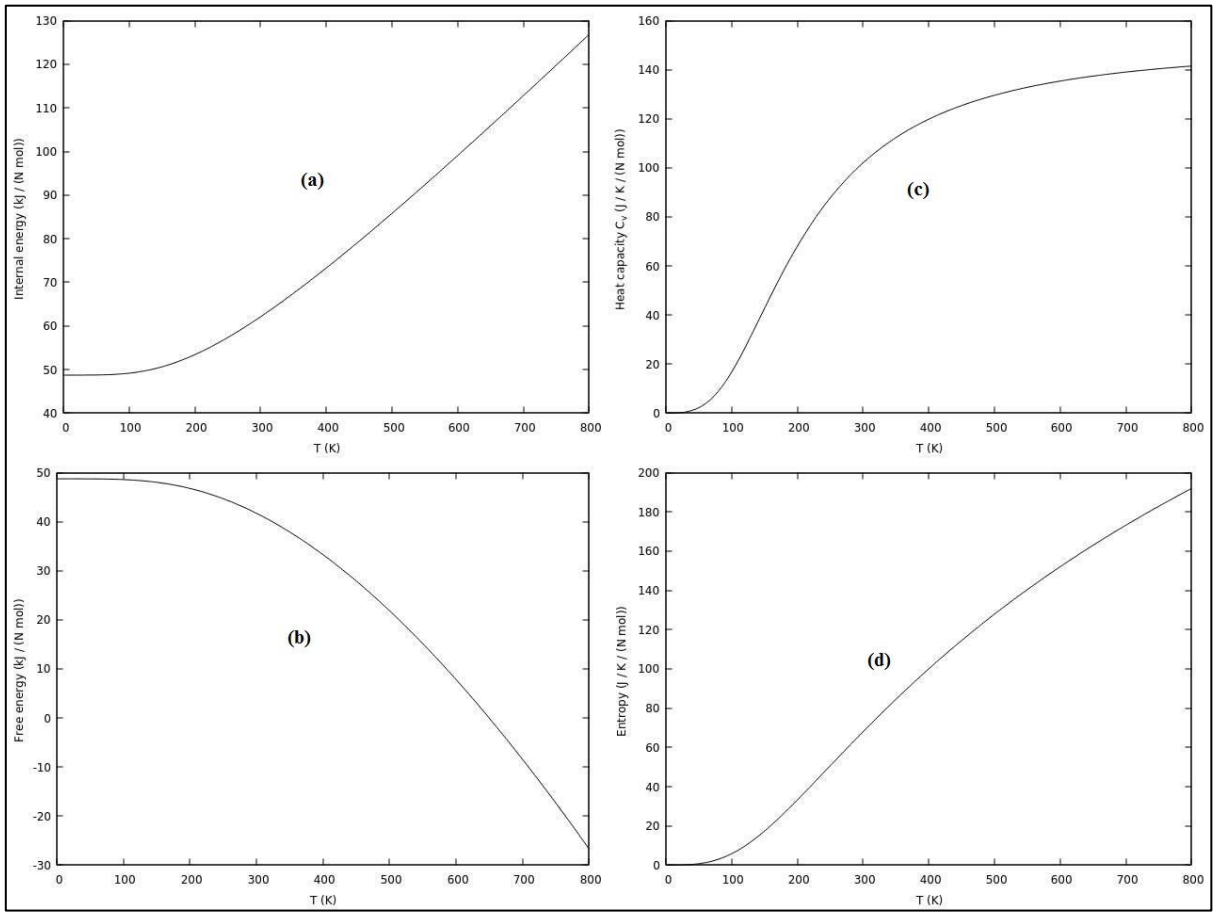

Figure 3: Dependence of **(a)** Internal energy, **(b)** Free energy, **(c)** Heat capacity and **(d)** Entropy of $C11_b - CrSi_2$ alloy on temperature from (0 – 800) K

Table 2: Density ρ, minimum thermal conductivity k_{min}, specific heat capacity C_V at 300 K, zero-point energy E_Z , Debye temperature θ_D, and the compressional, bulk, shear and average sound velocities of the $C11_b - CrSi_2$ alloy. The result in parenthesis **(a)** is from (Pan, 2020)

Material	ρ (g/cm^3)	k_{min} (mW/K–m)	C_V (J/K.mol)	E_Z (kJ/N.mol)	θ_D (K)	V_C (m/s)	V_B (m/s)	V_S (m/s)	V_{Avg} (m/s)
$C11_b$-$CrSi_2$	5.34	17.43	142.13	48.73	867.87	9328.45	6279.38	5974.28	6525.41
	5.04[(a)]	-	-	-	624.4[(a)]	-	-	-	-

3.3 Optical Properties

Optical properties play active role in the understanding of the nature of materials and can give a clear picture of the material usage in optoelectronic devices. Dielectric function as the bridge of microphysics, can process inter-band electronic transitions, the nature of electrons in solids, as well as the reflection of the energy band structure of solids and other spectrum information. Generally, the interaction of a photon with electrons within the material can be described in terms of time-dependent perturbations of the electronic ground states. The transitions between the occupied and unoccupied states originate mainly from the photon's electric field. The photon excitations yielding the spectra are described by the joint density of states (J-DOS) between the conduction and valence bands. A material's response to an electromagnetic field is described by means of the complex dielectric tensor given blow in equation 13:

$$\varepsilon(\omega) = \varepsilon_1(\omega) + i\varepsilon_2(\omega) \qquad (13)$$

where $\varepsilon_2(\omega)$ and $\varepsilon_1(\omega)$ are the imaginary and real frequency-dependent parts of dielectric tensor, respectively. Moreover, the imaginary part $\varepsilon_2(\omega)$ can be obtained directly using the knowledge of inter-band transitions from the

electronic band structure and related absorptive treatment. The real part $\varepsilon_1(\omega)$ of the dielectric tensor is an extraction from the $\varepsilon_2(\omega)$ using Kramers-Kronig (K-K) formalism and it is expressed as:

$$Im\varepsilon_2(\omega) = \frac{1}{\pi}\left[\frac{\hbar e}{m\omega}\right]^2 \sum_{c,v'} \int dk \langle c_k|P^{\alpha}|v_k\rangle\langle v_k|P^{\beta}|c_k\rangle \times \delta\left(\varepsilon_c^k - \varepsilon_v^k - \omega\right) \quad (14)$$

where 'v' and 'c', respectively denote valance and conduction bands in basis sets and energies in the Kronecker delta, and e, ω, Prespectively denote the electric charge, light frequency, and momentum operator in α and β directions. The real part obtained using K-K formalism is given by:

$$\mathrm{Re}\,\varepsilon_1(\omega) = \delta_{\alpha\beta} + \frac{2}{\pi} P\int_0^{\infty} d\omega' \frac{\omega' \mathrm{Im}.\varepsilon_2(\omega')}{(\omega')^2 - \omega^2} \quad (15)$$

and it describes the electronic polarizability of the material. Accordingly, the crystal symmetry of the dielectric tensor can have up to three components (xx ≠ yy ≠ zz) as depicted in Figures 5 ((a) and (b)).

Figures 4 and 5, show the optical dependence of the joint density of states (Joint-DOS), the imaginary part of dielectric function $[\varepsilon_2(\omega)]$ and the real part of dielectric function $[\varepsilon_1(\omega)]$ of the photon energy grid for the $C11_b - CrSi_2$. Using the calculated lattice parameters from the electronic properties of the alloy is deployed to compute the electronic joint density of states (Joint-DOS) which is presented as shown in Figure 4. The transitions between occupied and unoccupied states alongside single-particle excitations emanate usually due to the electric field, and yield resulting spectra known as Joint-DOS between the valence-band and conduction-band (Adolph *et al*., 1997). The Joint-DOS curve due to shifted energies is subdivided into several regions, first between 1 and 2 eV, the curve has a peak at 1.96 eV. In addition, between 3.0 eV and 5.0 eV, two predominant peaks are clearly seen at about 3.5 eV and 5.0 eV respectively. At higher energies, there exist several lower peaks due to attenuating oscillatory strength, and eventually go to zero at about 16.7 eV. Further, the DFT method adopted in this analysis is highly accurate, stemming from its reliance on quantum ab-initio formalism. However, the calculation only depicts energy shifts up to 20 eV for the considered electromagnetic spectrum as accurate. Meanwhile, outside the given energy range, it has been established in other alloys (Adebambo *et al*., 2010) that at elevated energies, incorrect bands as well as a reduction in refractive index below unity may occur owing to artifacts in calculations.

In Figure 5(a), the imaginary part of dielectric function $\varepsilon_2(\omega)$ is as depicted. The majority peaks within 0.96 eV to 5.47 eVare predominantly of the transitions from the Si 2p-states in the valence-band to the Cr 3d-states in the conduction-band. At higher energy of about 6.0 eV, other peaks originate from the transitions from Si 2s-level to the conduction-band. The transition energies are observed to be in the energy range of the ultraviolet spectrum. The pronounced frequency dependence and the anisotropic effect of the dielectric function in $C11_b - CrSi_2$ are clearly indicative interplay between the matrix elements and the Joint-DOS effects. The anisotropic effect is predominantly due to strong variation in optical matrix components. The pronounced splitting of the peaks into two characteristic regions at lower and higher energies which are separated by minima around the photon energy of circa 6 eV are found to exhibit the same trend as in the Joint-DOS of Figure 4. This behavior of the imaginary part of dielectric function mimicking the Joint-DOS spectra reflects the accuracy of the calculations.

Figure 5(b) depicts the frequency-dependent

dielectric function of the real part for the $C11_b - CrSi_2$ alloy. The real part of the material's dielectric function $\varepsilon_1(\omega)$ is plotted in three directions (x, y, z) up to 20 eV. The nature of the curve depicts that the real part of dielectric function of each component lies above the zero-point of the vertical profile. Consequently, from Figure 5(b), it is clear that there is relatively high anisotropy in the three directions. At zero-energy, the static dielectric constants $\varepsilon_1(0)$ are 17.15, 38.77 and 47.84 in the x, y and z directions, respectively. Generally, below the Fermi energy, materials with negative dielectric constants are expected to exhibit a metal-like behavior while those with a positive dielectric value $(\varepsilon_1(\omega) > 0)$ are usually dielectric in nature. The observed minimum values of the real part of Epsilon along the three directions x, y and z respectively are positive within the energy grid. This trend suggests that the material can exhibit strong dielectric characteristics. Refractive index $n(\omega)$ can describe the nature of photon propagation inside a material, and it exemplifies the real part of the complex refractive tensor. Additionally, to evaluate its value at zero-energy, the knowledge of the square root of $\varepsilon_1(0)$ is assumed (i.e.,$n^2(0) = \varepsilon_1(0)$). From Figure 5(b), the static refractive index$n(0) = 4.14\,, 6.23,\ 6.92$for x-, y- and z-components. The refractive index decreases with the increase of photon energy. Accordingly, the refractive index is links to the dielectric function as $n^2(\omega) - k^2(\omega) = \varepsilon_1(\omega)$ and $2n(\omega)k(\omega) = \varepsilon_2(\omega)$ respectively, where $k(\omega)$ is the extinction coefficient. From Figure 5(a), it can be seen that the extinction coefficient $k(\omega)$ of tetragonal $CrSi_2$ will be zero below 0.47 eV and above 14.1 eV. When the photon energy is circa 0.96 eV, $k(\omega)$gets its maximum values. Clearly, the extinction coefficient $k(\omega)$decreases with increasing photon energy above 0.96 eV, and reaches zero when the photon energy is 14.1 eV. Consequently, the imaginary part of the dielectric function is relative to the absorption coefficient; hence, the extinction coefficient at the same time shows great absorption characteristics at the band-edge. In Figure 6, the anisotropic effect exhibited in the static refractive index calculations is clearly seen, and it is a show of the material's application to birefringence.

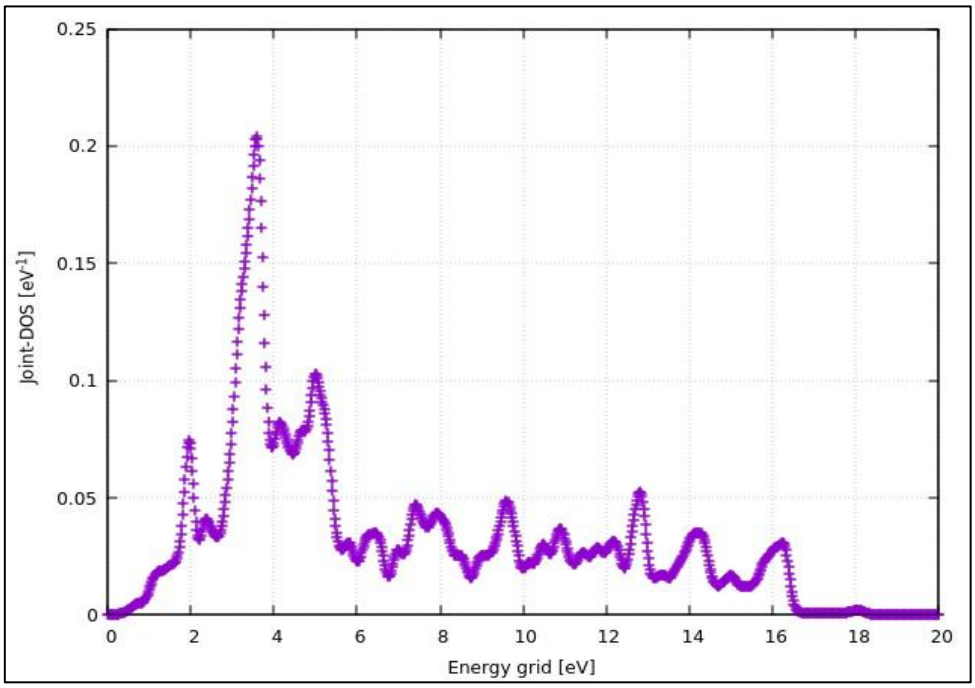

Figure 4: A plot of electronic joint density of states as a function of energy grid

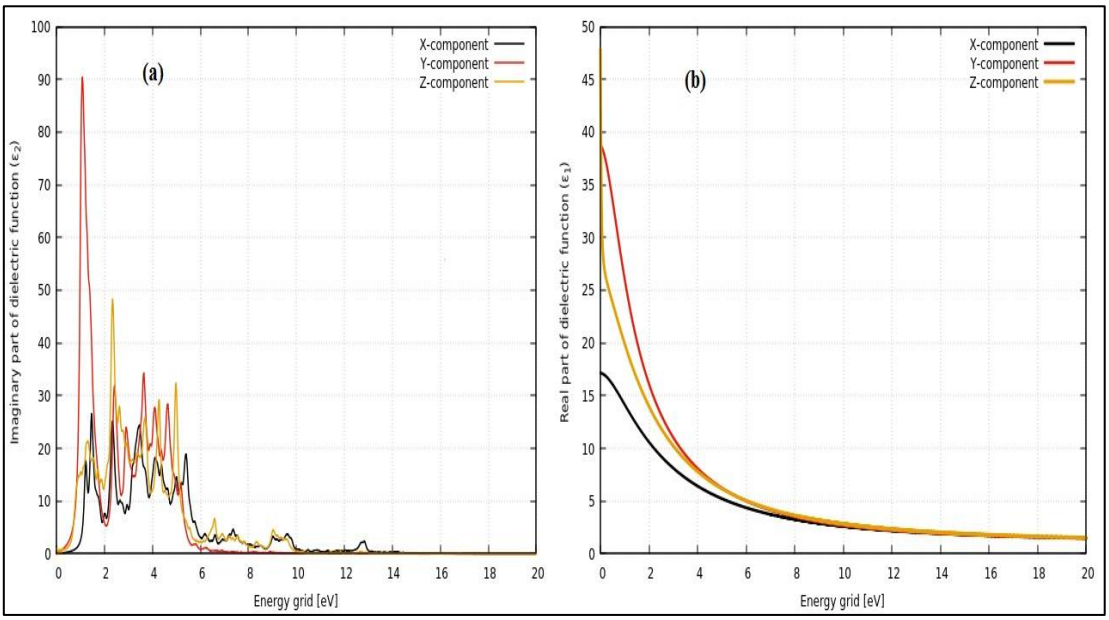

Figure 5: **(a)** Imaginary part of dielectric function curve while **(b)** Real part of dielectric function for$C11_b - CrSi_2$ alloy

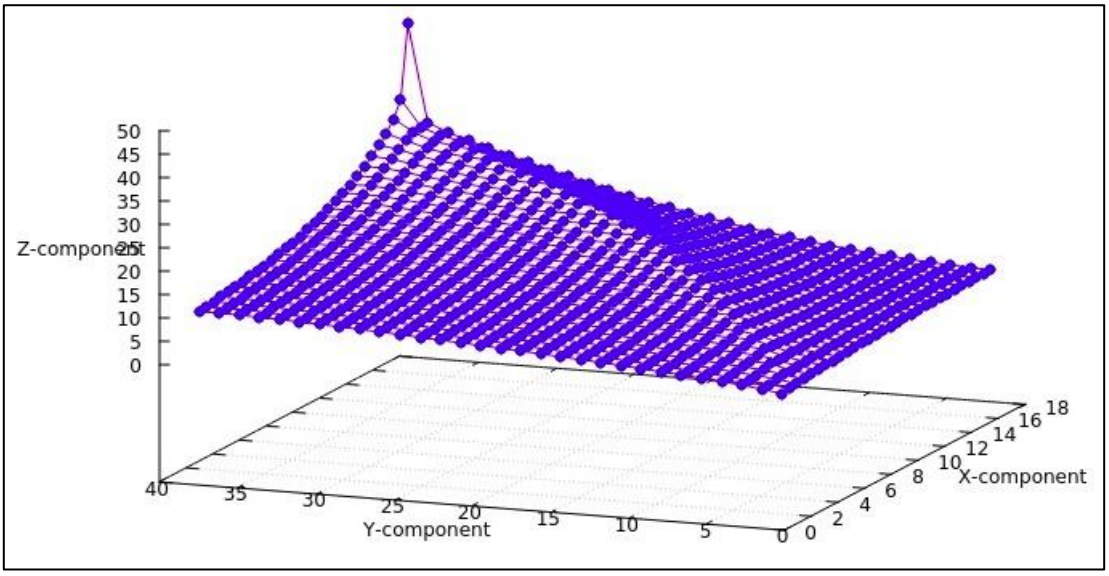

Figure 6: Anisotropic effect in x-, y- and z-directions of tetragonal $C11_b - CrSi_2$ material

5.0 Conclusion

In this study, investigation of the structural, electronic, thermo-physical, and optical properties of tetragonal $C11_b - CrSi_2$ structure has been carried-out using the first-principles density functional theory (DFT) method based on the plane-wave pseudo-potential theory. The lattice optimization performed in this study shows good agreement with the experimental result. The ground state parameters as well as the thermodynamic and optical properties of the tetragonal $C11_b - CrSi_2$ material are calculated and analyzed using the framework of DFT as implemented in the Quantum Espresso code. All results of the calculated ground state parameters obtained from the *E-V* data agree well with the experiment. The band structure and density of state (DOS) show a metallic

nature of $C11_b - CrSi_2$ structure. The calculated DOS around the Fermi level is 3.61 per eV. Our study shows that the internal energy and the entropy increase monotonously with increasing temperature *T*, while the free energy decreases with rising temperatures. The constant volume heat capacity C_V increases exponentially with temperature for T < 400 K, while for high temperatures all phonon modes are sufficiently excited by the thermal energy, rendering C_V approaches the Dulong-Petit limit. A Dulong-Petit limit of142.13 J/(mol·K) was observed for the Cv. The high specific heat capacity reveals the materials absorptiveness to heat. Its thermodynamic properties reflect the readiness of the $C11_b - CrSi_2$ as a high temperature material. The optical dielectric properties, such as imaginary and real parts of dielectric function, static refractive index, and extinction coefficient, reveals relatively high anisotropy and show great absorption at band-edge.

Conflicts of Interest

The authors declare no conflicts of interest regarding the publication of this article.

References

Adachi, S., (2005). Properties of Group-IV, III–V and II–VI Semiconductors (New York: Wiley, 2005).

Adebambo, P.O., Bamgbose, K.M, Olowofela, J.A., Oguntuase, J.A., Adebayo, G.A., (2010). Electronic structure and optical properties of α –Fe–Al alloy from ab initio calculations. *Physica B* 405: 4578–4581. https://doi.org/10.1016/j.physb.2010.08.043

Adolph, B., Tenelsen, K., Gavrilenko, V.I., Bechstedt, F., (1997). Optical and loss spectra of SiC polytypes from *ab initio* calculations. *Phys. Rev.* B 55 (3): 1422. https://doi.org/10.1103/PhysRevB.55.1422

Anderson, O. L., (1963). A simplified method for calculating the Debye temperature from elastic constants. *J. Phys. Chem. Solids*, 24 (7), 909–917. https://doi.org/10.1016/0022-3697(63)90067-2

Bellani V., Guizzetti G., Marabelli F., Piaggi, A., Borghesi, A., Nava, F., Antonov, V. N., Antonov, Vl. N., Jepsen, O., Andersen, O. K., Nemoshkalenko, V. V., (1992). Theory and experiment on the optical properties of $CrSi_2$. *Phys. Rev. B*, 46: 9380 — 9389. https://doi.org/10.1103/PhysRev-B.46.9380

Bioud, N., Kassali, K., Bouarissa, N., (2017). Thermodynamic Properties of Compressed CuX (X = Cl, Br) Compounds: Ab Initio Study, *J. Electron Mater.*, 46, pp.2521. https://doi.org/10.1007/s11664-017-5335-x

Birch, F., (1978). Finite strain isotherm and velocities for single-crystal and polycrystalline NaCl at high pressures and 300°K. *J. Geophys. Res.*: *Solid Earth*, 83: 1257–1268. https://doi.org/10.1029/JB083IB03P01257

Cheng, C-H., Lien, Y-C., Wu, C-L., Lin, G-R., (2013). Multicolor electroluminescent Si quantum dots embedded in SiO_X thin film MOSLED with 2.4% external quantum efficiency, *Optics Express*, 21(1), pp. 391 – 403. https://doi.org/10.1364/OE.21.000391

Clarke, D.R., (2003). Materials Selection Guidelines for Low Thermal Conductivity Thermal Barrier Coatings. *Surf. Coat. Technol.*, 163–164, 67–74. https://doi.org/10.1016/S0257-8972(02)00593-5

Courtel, F. M., Duguay, D., Lebdeh, Y. A., Davidson, I. J., (2012). Investigation of CrSi2 and MoSi2 as anode materials for lithium-ion batteries. J. Power Sources, 202, 269–275. https://doi.org/10.1016/j.jpowsour.2011.11.047

Danilov F.I., Protsenko V.S., Gordiienko V.O., Kwon S.C., Lee J.Y., Kim M., (2011). Nanocrystalline hard chromium electrodeposition from trivalent chromium bath containing carbamide and formic acid: Structure, composition, electrochemical corrosion behavior, hardness and wear characteristics of deposits. *Appl. Surf. Sci.*, 257: 8048–8053. https://doi.org/10.1016/-j.apsusc.2011.04.095

Ekong, S. A., Fuwape, I.A., Odo, E.A., (2014).Ab initio study of the electronic structure ofsilicon quantum dots. *J. Nig. Assoc. Math.Phys*., 26: 177 – 186.

Ekong, S.A., Oloye, M.T., Oyegoke, D.A., (2015). Ground-state energy calculation of helium atom using quantum Monte Carlo casino-code, *Adv. Phys. Theo. Appl*., 46: 1 - 6.

Ekong, S.A., Osiele, M. O., (2016). A Quantum Confinement Study of the Electronic Energy of Some Nanocrystalline Silicon Quantum-Dots, *Intl. Lett. Chem. Phys. Astron.*, 63: 106 – 110. https://doi.org/10.18052-/www.scipress.com/ILCPA.63.106

Galkin, N. G., Velichko, T. A., Skripka, S. V., *et al.* (1996). Semiconducting and structural properties of $CrSi_2$ A-type epitaxial films on Si (111). *Thin Solid Films*, 280: 211–220.

Ghoranneviss M., Sari A.H., Esmaeelpour M., (2004). Nitrogen implantation and heat treatment effect on the hardness improvement of the chromium film surface deposited on Si (1 1 1) substrate. *Appl. Surf. Sci*., 237: 326–331. https://doi.org/10.1016-/S0169-4332(04)00981-X

Giannozzi, P., Baroni, S., Bonini, N., Calandra, M., Car, R., Cavazzoni, C., Ceresoli D., Chiarotti, G. L., Cococcioni, M., Dabo, I.,*et al*. (2009). "QUANTUM ESPRESSO: a modular and open-source software project for quantum simulations of materials." *Journal of physics: Condensed matter* 21 (39): 395502. https://doi.org/10.1088-/0953-8984/21/39/395502

Gregory, E. E., Ekong, S. A., Emah, J. B., (2024). Ab-initio Assessment of the Electronic, Mechanical, Thermal, Optical and Phonon Properties ofB3-AlAs, *Res. J. Sci. Technol*., 4(3): 69 – 93.

Han, N., Liu, H., Zhao, J., (2015). Novel Magnetic Monolayers of Transition Metal Silicide. *J. Supercond. Nov. Magn*., 28(6), 1755–1758. https://doi.org/10.1007/-s10948-014-2940-2

He, J., Guo, X., Qiao, Y., (2020). Oxidation behavior and adhesion performance of $TiSi_2$-$NbSi_2$ composite coating prepared via magnetron sputtering and then pack cementation. *J. Alloys Compd*., 820, 153425. https://doi.org/10.1016/j.jallcom-.2019.153425

Jong, J.-Y., Zhu, J., Pak, S.-I., Sim, G.-H., (2016). Theoretical Investigation of Mechanical, Electronic, and Thermal Properties of Fe_2TiSi and Fe_2TiSn under Pressure. *J. Electron. Mater*. 45: 5104–5111. https://doi.org/10.1007/s11664-016-4722-z

Kondo, S-i., Hasaka, M., Morimura, T., Miyajima, Y., (1994). Mössbauer effect of Co- or Mn-doped β-$FeSi_2$, *Physica B*, 198(4), 332–336. https://doi.org/10.1016-/0921-4526(94)90021-3

Krijn, M. P. C. M., Eppenga R., (1991). First-principles electronic structure and optical properties of $CrSi_2$. *Phys. Rev. B*, 44: 9042 — 9044. https://doi.org/10.1103/PhysRev-B.44.9042

Lebga, N., Daoud, S., Sun, X-W, Bioud, N., Latreche, A.,(2018). Mechanical and Thermophysical Properties of Cubic Rock-Salt AlN under High Pressure,*J. Electron. Mater*. 47: 3430–3439. https://doi.org/-10.1007/s11664-018-6169-x

Lin Y.C., Hsu C.Y., Hung S.K., Chang C.H., Wen D.C., (2012). The structural and optoelectronic properties of Ti-doped ZnO thin films prepared by introducing a Cr buffer layer and post-annealing. *Appl. Surf. Sci.*, 258: 9891–9895. https://doi.org/10.-1016/j.apsusc.2012.06.046

Lu, Y., Duan, Y., Peng, M., Yi, J., Li, C., (2021). First-principles calculations of electronic, optical, phononic and thermodynamic properties of C40-type TMSi2 (TM = Cr, Mo, W) disilicides. *Vacuum*, 191, 110324. https://doi.org/10.1016/j.-vacuum.2021.110324

Maier-Flaig, F., Rinck, J., Stephan, M., Bocksrocker, T., Bruns, M., Kübel, C., Powell, A. K., Ozin, G. A., Lemmer, U., (2013). Multicolor silicon light-emitting diodes (SiLEDs), *ACS Nano-letters*, **13** (2), pp. 475 – 480. https://doi.org/-10.1021/nl3038689

Malica, C., Corso, A.D., (2020). Quasi-harmonic temperature dependent elastic constants: applications to silicon, aluminum, and silver. *J. Phys. Condens. Matt.*, 32. https://doi.org/10.1103/PhysRevB.-55.14422

Malica, C., Dal Corso, A., (2020). Temperature dependent elastic constants and thermodynamic properties of BAs: An ab initio investigation. *J. Appl. Phys*., 127, 245103-1 – 245103-6. https://doi.org/10.1063-/5.0011111

Mattheiss, L.F., (1992). Calculated structural properties of $CrSi_2$, $MoSi_2$, and WSi_2. *Phys. Rev*. B: *Condens. Matter Mater. Phys*. 45(7), 3252–3259. https://doi.org/10.1103/physrevb.45.3252

Mesbah, S., Houari, M., Boufadi, F.Z., Bouadjemi, B., Lantri, T., Bentata, S., Ameri, M., (2021). Full Heusler alloys, with high absorption coefficient, insight into the optical properties of Li_2CaC and Li_2SrC, *Sol. Stat. Comm.*, 328, 114238. https://doi.org/10.1016/j.ssc.2021.114238

Monkhorst, H.J., Pack, J.D., (1976). Special points for Brillouin-zone integrations, *Phys. Rev.* B, 13, pp.5188–5192. https://doi.org/10.1103/PhysRevB.13.5188

Mousa, A. M., Jawad, K. H., (2015). Performance of a Nano PbS/Si Hetrojunction deposited by chemical spray pyrolysis, *Intl. Lett. Chem. Phys. Astron.*, 51: 13 – 16. https://doi.org/*10.56431/p-4f9xb7*

Murnaghan, F.D., (1944). The compressibility of media under extreme pressures, *Proc.Natl. Acad. Sci.* 30 (9). http://dx.doi.org/10.1073/pnas.30.9.244

Pan, Y., (2020a). Structural prediction and overall performances of $CrSi_2$ disilicides: DFT Investigations. *ACS Sustainable Chem. Eng.*, 8, 11024−11030. https://dx.doi.org/10.1021/acssuschemeng.0c04737

Pan, Y., (2020b). First-principles investigation of structural, electronic, and optical properties of transition metal-doped C40 $CrSi_2$. *Intl. J. Quantum Chem*., e26401. https://doi.org/10.1002/qua.26401

Pan, Y., Li, Y., Zheng, Q., (2019). Influence of Ir concentration on the structure, elastic modulus and elastic anisotropy of Nb Ir

based compounds from first-principles calculations. *J. Alloys Compd.*, 789, 860−866. https://doi.org/10.1016/j.jallcom.2019.03.083

Pan, Y., Mao, P., Jiang, H., Wan, Y., Guan, W., (2017). Insight into the effect of Mo and Re on mechanical and thermodynamic properties of $NbSi_2$ based silicide. *Ceram. Intl*., 43(6), 5274 – 5282. https://doi.org/10.1016/j.ceramint.2017.01.055

Santoni F., Giovine E., Torrioli G., Chiarello F., Castellano M.G., (2014). Study of the Fabrication Process for a Dual Mass Tuning Fork Gyro. Procedia Eng., 87: 991–994. https://doi.org/10.1016/j.proeng.2014-.11.325

Shin, Y., Rhim, S. H., Duong, A. T., Nguyen, V. Q., Hong, S. C., Cho, S., Park, H-M., (2015). New synthesis of $MnSi_2$ thin film and its thermoelectric properties. *J Vac. Sci. Technol.* A 33(6), 061516. http://dx.doi.org/10.1116/1.4932515

ShiYun, Z., Quan, X., WanJun, Y., Qian, C., (2009). First-principles study on the electronic structure and optical properties of $CrSi_2$. *Sci. China Ser. G: Phys. Mech. Astron*., vol. 52, no. 1, 46–51. https://doi.org/10.1007/s11433-009-0003-7

Vanderbilt, D., (1990). Soft self-consistent pseudopotentials in a generalized eigenvalue formalism, *Phys. Rev.* B, 41, pp. 7892(R). https://doi.org/10.1103/PhysRevB.41.7892

Vasudévan, A.K., Petrovic, J.J. (1992). A comparative overview of molybdenum disilicide composites., *Mater. Sci. Engr.*, A 155(1-2), 1–17. https://doi.org/10.1016-/0921-5093(92)90308-n

Wan, B., Xiao, F., Zhang, Y., Zhao, Y., Wu, L., Zhang, J., Gou, H.,, (2016). Theoretical study of structural characteristics, mechanical properties and electronic structure of metal (TM=V, Nb and Ta) silicides. *J. Alloy. Compd*., 681, 412 – 420. https://doi.org/10.1016/j.jallcom.2016.04.253

Wang X., Chen F., Liu H., Liang W., Yang Q., Si J., Hou X., (2009). Fabrication of micro-gratings on Au-Cr thin film by femtosecond laser interference with different pulse durations. *Appl. Surf. Sci*., 255: 8483–8487. https://doi.org/10.1016-/j.apsusc.2009.06.057

Xiong, H., Gan, L., Li, M., (2020). Improving the oxidation resistance of WSi_2 by boron doping: A DFT study. *Mater. Today Commun*., 25, 101312. https://doi.org/-10.1016/j.mtcomm.2020.101312

Yakaboylu, G. A., Yumak, T., Sabolsky, K., Sabolsky, E. M., (2020). Effect of high temperature preoxidation treatment on the oxidation behavior of $MoSi_2$- and WSi_2-Al_2O_3 composites. *J. Alloys Compd*., 816, 152499. https://doi.org/10.1016/j.jallcom-.2019.152499

Yate A.L., Mart L., Esteve J., Lousa A., (2017). Ultra Low Nanowear in Novel Chromium/Amorphous Chromium Carbide. *Appl. Surf. Sci*., 420, 707–713.https://doi.org-/10.1016/j.apsusc.2017.05.203

Zhou, S.G., Tian, M.L, Xu, Y., Zhang, C., Cao, Y., (2022). First-principles study of the elastic, thermal and optical properties of α-PbO_2 and β-PbO_2.*Indian J. Phys.*, 96, pp.3449–3460. https://doi.org/10.1007-/s12648-022-02305-3